Electronic Supplementary Material (ESI) for Journal of Materials Chemistry A.

Supporting Information

Ultrathin Pt-Pd Nanosheets for Enhanced Formic Acid Oxidation and Oxygen Reduction Reaction

Qian Yang, [a] Lijie Shi, [a] Beibei Yu, [a] Jun Xu, [b] Cong Wei, [c] Yawen Wang*[a] and Hongyu Chen*[a]

a Institute of Advanced Synthesis, School of Chemistry and Molecular Engineering, Jiangsu National Synergetic Innovation Center for Advanced Materials, Nanjing Tech University, Nanjing, 211816, P. R. China.

b Department of Physics, Research Institute for Biomimetics and Soft Matter, Fujian Provincial Key Laboratory for Soft Functional Materials, Xiamen University, Xiamen, 361005, China

c Key Laboratory of Flexible Electronics (KLOFE) & Institute of Advanced Materials (IAM), Jiangsu National Synergetic Innovation Center for Advanced Materials (SICAM), Nanjing Tech University, Nanjing, 211816, P. R. China.

Section S1. Chemicals

All materials were obtained from commercial suppliers and used without further purification. Chloroplatinic acid hexahydrate ($H_2PtCl_6 \cdot 6H_2O$, ≥37.50% Pt basis), Sodium tetrachloropalladate(Na_2PdCl_4), Pd black and Nafion (5%) were purchased from Sigma Aldrich. Commercial Pt/C (20 wt%) and Pt black were purchased from Johnson Matthey. Potassium hydroxide, ethylene glycol (EG), ethanol Sulfuric acid, and N,N-dimethylmethanamide (DMF) were purchased from Sinopharm Chemical Reagent Co. Ltd. (Shanghai, China). Diethylenetriamine and Formic acid were purchased from Energy Chemical. Deionized (DI) water from Milli-Q System (Millipore, Billerica, MA) was used in all our experiments.

Section S2. Synthesis

Synthesis of Pt-Pd nanosheets. In a typical synthesis, 100 μL H_2PtCl_6(8 wt%), 100 μL Na_2PdCl_4(4.54 wt%) and 1 g of potassium hydroxide (KOH) were dissolved in a mixed solvent of 6 mL of N, N-dimethylformamide (DMF), 4 mL of ethylene glycol (EG) and 5 mL of diethylenetriamine (DETA) by sonication. The homogeneous reaction solution was then transferred to a 25 ml Teflon-lined stainless-steel autoclave, and heated at 200 ˚C for 2 h. The as-obtained nanosheets were washed with ethanol for four times, and then dried in an 80 ˚C oven overnight. Pt-Pd alloy nanosheets with other Pt/Pd atomic ratios can be obtained by using same synthetic method with different amount of H_2PtCl_6.

Section S3. Electrochemical Characterization

Formic acid oxidation reaction (FAOR) tests. All FAOR experiments were conducted on the electrochemical workstation (CHI 1040C) in a conventional three-electrode system at room temperature. The glassy carbon electrode (GCE, 3 mm diameter, 0.07065 cm^2) as the working electrode, saturated calomel electrode (SCE) as the reference electrode, and Pt wire as the counter electrode. Prior to use, the GCE was carefully polished by Al_2O_3 slurry and washed with ethanol and deionized water in an ultrasonic bath. The suspension of Pt-Pd alloy nanosheets (1 mg/mL) was dropped onto the GCE with the total metal loading of 4 μg. After the solvent evaporation under room temperature, the electrode was covered with nafion (2 μL, 0.5 wt%) in ethanol and dried at the air for 0.5h. For commercial Pt/C, Pt black or Pd black, 4 μL suspension of Pt/C (20 wt% Pt nanoparticles supported on carbon black, 5 mg/mL), Pt black (1 mg/mL) or Pd black (1 mg/mL) was transferred onto GCE, the loading of metal was 4 μg. The cyclic voltammograms (CVs) were recorded in nitrogen-saturated 0.5 M H_2SO_4 solution, and the potential was scanned from -0.241 to 1 V (vs SCE) at a scan rate 50 mV s^{-1}. The scan was repeated several times to ensure that a stable cyclic voltammetry (CV) was obtained. Voltammogram measurements for formic acid oxidation were carried out in fresh made 0.5 M H_2SO_4+0.25 M formic acid solution, and the potential was scanned from -0.2 to 1V (vs SCE) at a scan rate 50 mV s^{-1}. The stability was evaluated by chronoamperometry at 0.05V (vs SCE) for 3600 s in fresh made 0.5 M H_2SO_4+0.25 M formic acid solution.

Oxygen reduction reaction(ORR) measurements. The ORR tests were carried out in 0.1 M KOH at room temperature through the Autolab electrochemistry station using a glassy-carbon rotating disk electrode (diameter: 5 mm, area: 0.196 cm^2) as the working electrode to load a thin catalyst film. Saturated calomel electrode (SCE) as the reference electrode, and Pt plate as the counter electrode. All the potentials were transferred to a reversible hydrogen electrode (RHE) by adding a value of 1.0116. To prepare the working electrode, the suspension of catalysts ($V_{isopropanol}$: V_{water}=1:2, $V_{5wt\%nafion}$=0.025 $V_{solvent}$, 1 mg/ml $_{metal}$) were obtained by ultrasonic mixing for about 2h. Then transferred 10 μl suspension to the RDE and dried at room temperature. For commercial Pt/C, 10 μl suspension of Pt/C (20 wt% Pt nanoparticles supported on carbon black, 5 mg/ml) was transferred onto RDE. For all catalysts, the loading of metal was 10 μg. The cyclic voltammograms (CVs) were obtained in nitrogen-saturated 0.1M KOH solution and the potential was scanned from -1 to 0.3 V (vs SCE) at a scan rate 50 mV s^{-1}. The scan was repeated several times to ensure that a stable cyclic voltammetry (CV) was obtained. All the ORR electrochemical measurements were carried out in N_2- versus O_2-saturated atmosphere at room temperature to eliminate the background current at a scan rate of 10 mV s^{-1} with the rotation rate of 1600 rpm. The stability of $Pd_{19}Pt_1$ was estimated by the accelerated durability test (ADT), which was carried out between 0.6 V and 1.0 V (versus RHE) at a scan rate of 200 mV s^{-1} for 10,000 cycles. The ORR polarization curves was recorded before ADT and after 10,000 cycles.

CO-stripping tests. The 0.5 M H_2SO_4 electrolyte solution was first bubbled with Ar for 30 min to remove O_2. Then the system was bubbled with CO for 30 min while keeping the potential at 0 V vs SCE for adsorbing CO on the electrode. The dissolved CO was removed by bubbling with Ar for another 30 min before carrying the cyclic voltammograms.

Section S4. Characterization

TEM images were collected from a HT7700 Transmission Electron Microscopy operated at 100 kV and a Talos L120C modeloperated at 120 kV. Field emission scanning electron microscopy (SEM) image were collected on a FEI Quanta 250 FEG. High resolution TEM image, HAAD-STEM and energy dispersive X-ray (EDX) mapping analyses were taken from a JEOL 2100F Transmission Electron Microscope operated at 200 kV. The compositions of the catalysts were determined by ICP-OES (Avio™ 200,

PerkinElmer). The XRD analysis was carried out on a Bruker D8 Advance X-ray diffractometer with Cu Kα radiation. XPS measurements were carried out with Thermo ESCALAB 250Xi spectrometer by using a monochrome Al Ka (1486.6 eV) X-ray source. All the spectra were calibrated to the binding energy of the C1s peak at 284.8 eV. The thickness of nanosheets was measured by atomic force microscopy (Dimension ICON with Nanoscope V controller, Bruker). Thermogravimetric analysis (TGA) was carried out under a flow of N_2 with a temperature ramp of 10 °C min^{-1} from room temperature to 600 °C. The Fourier-transform infrared spectroscopy (FT-IR) spectra were recorded from KBr disks using a ThermoFisher (NICOLET Is10) instrument in the wavenumber range of 4000 - 1000 cm^{-1}.

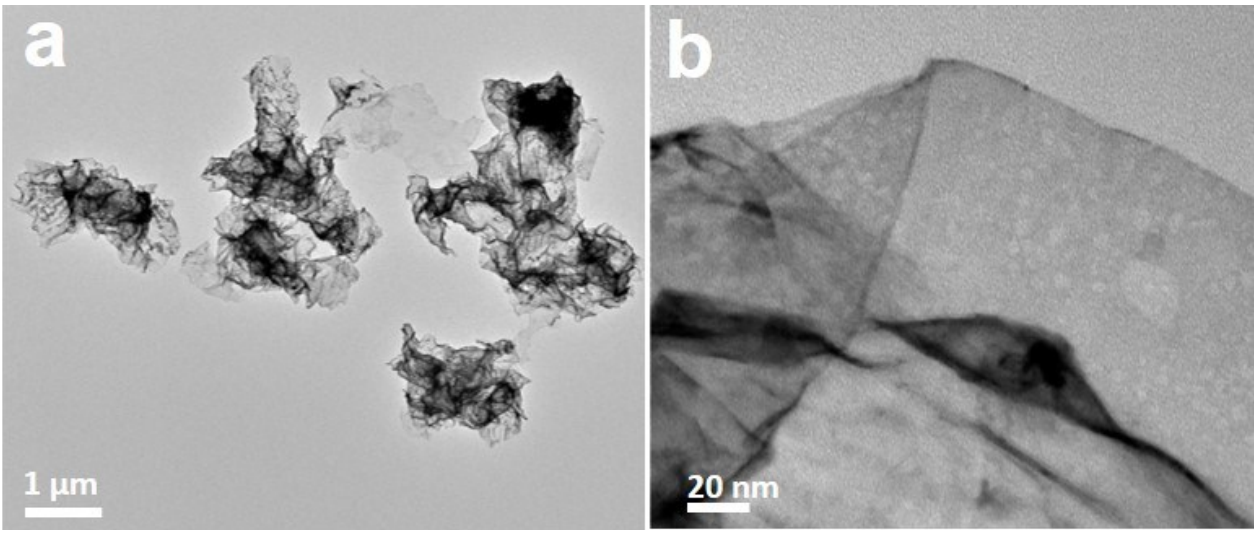

Fig. S1 The high-magnification TEM images of the as-prepared Pt-Pd allloy nanosheets.

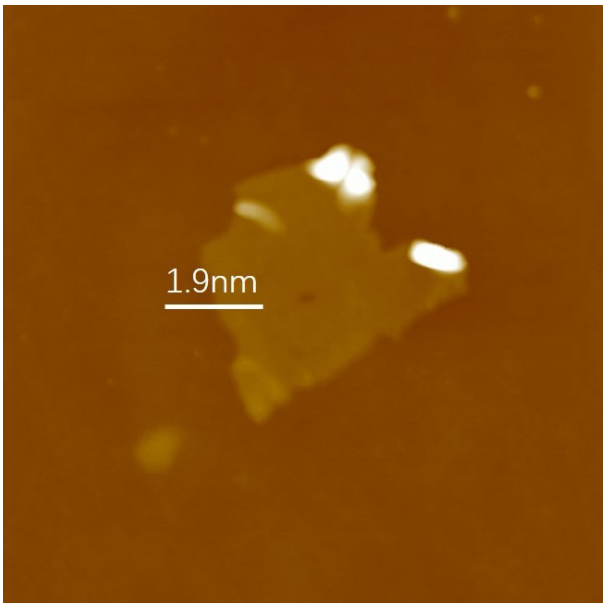

Fig. S2 Thickness measurement of Pt-Pd nanosheets by AFM. The measured thickness of nanosheets is about 1.9 nm.

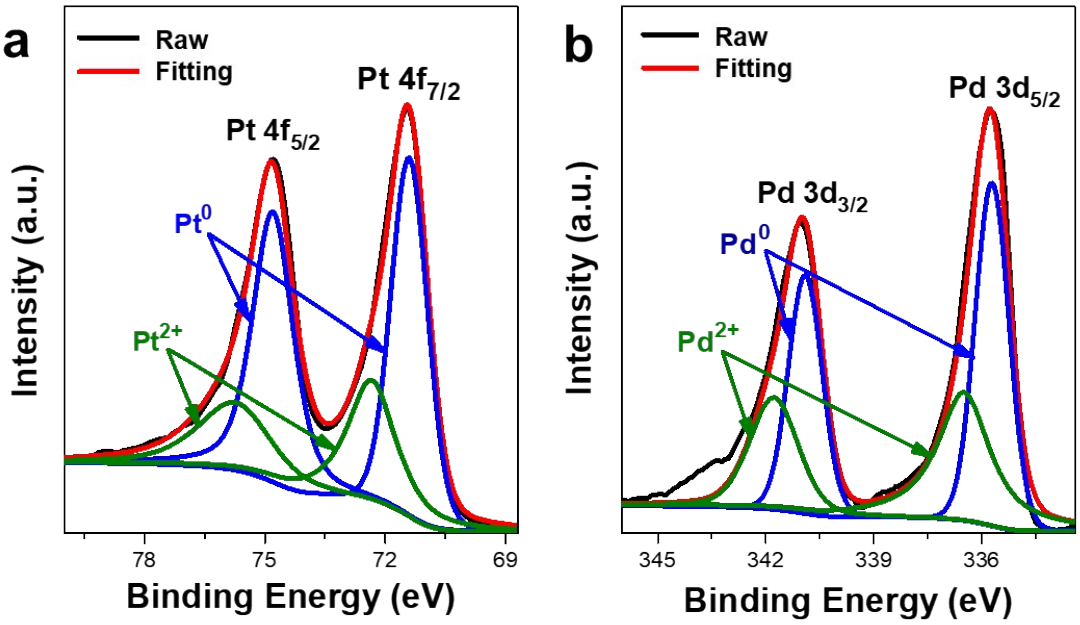

Fig. S3 a) Pt 4f, b) Pd 3d XPS spectra of the Pt-Pd nanosheets, respectively.

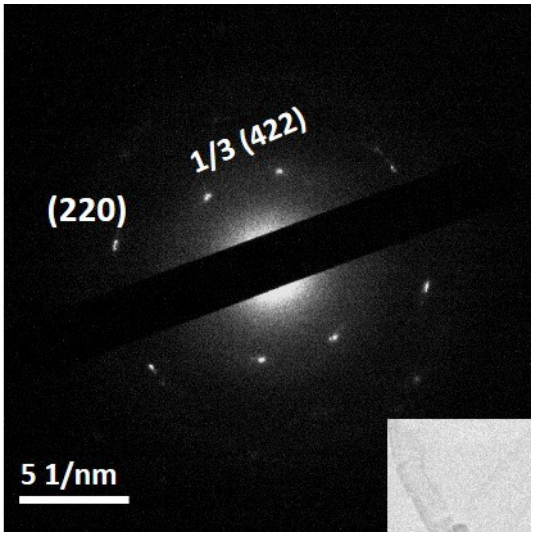

Fig. S4 SAED patterns of Pt-Pd nanosheets (shown in the inset).

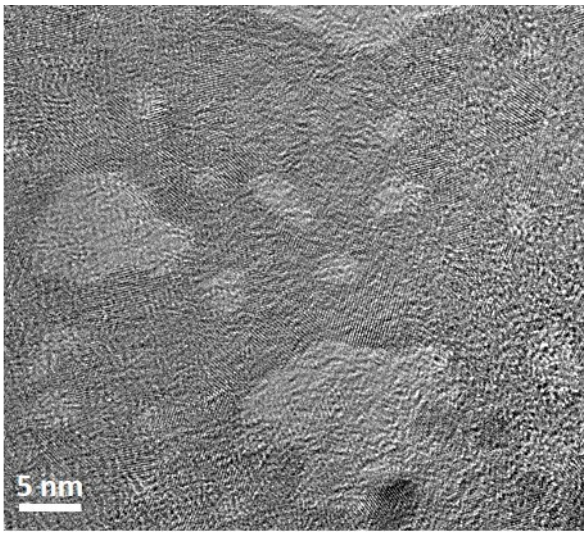

Fig. S5 The HRETM image of Pt-Pd alloy nanosheets upon irradiation by an electron beam.

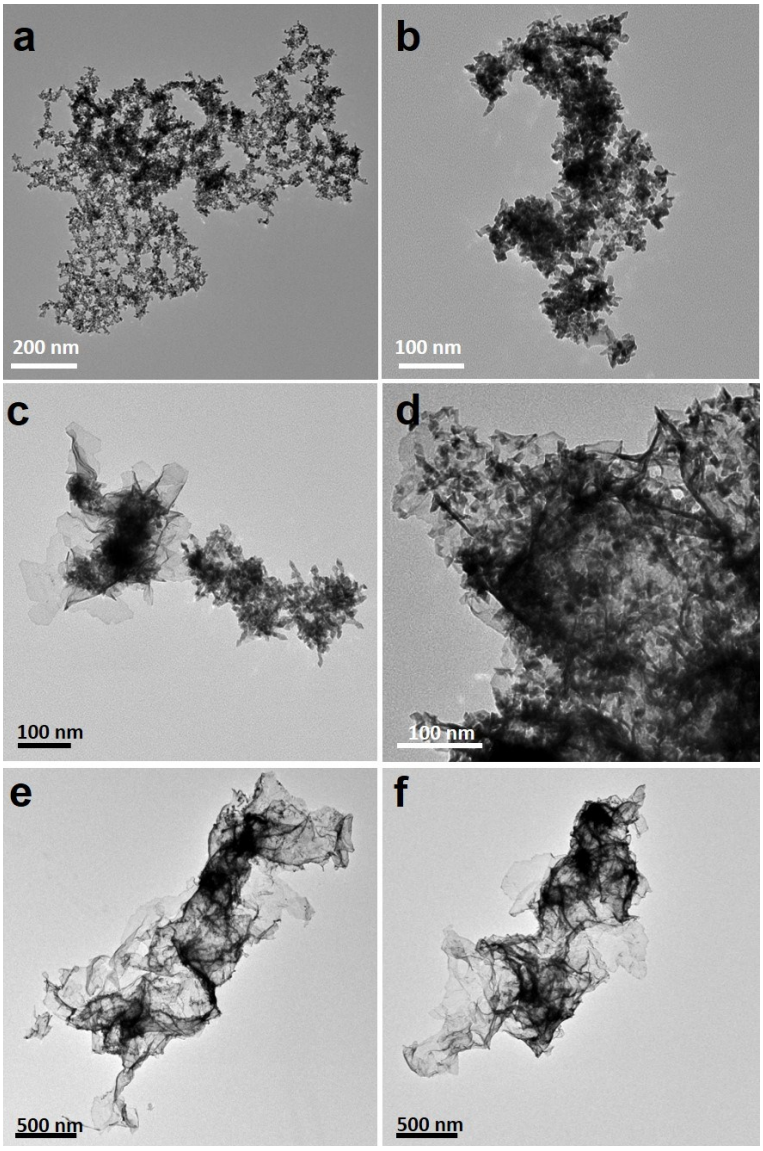

Fig. S6 TEM image of Pt-Pd nanosheets at different reaction time: a, b) 0 min; c, d) 20 min; e) 1h; f) 4h.

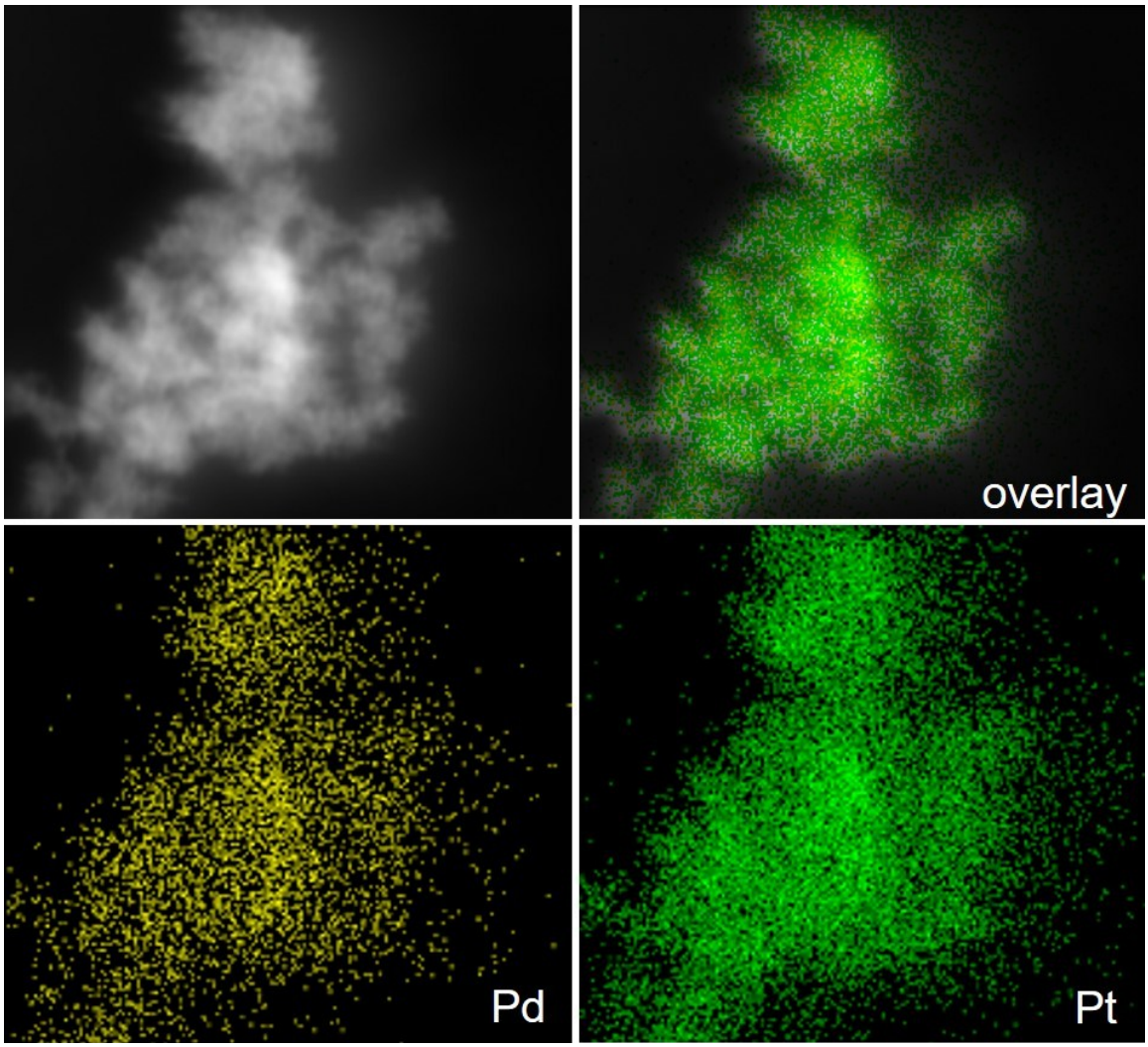

Fig. S7 HAADF-STEM image and the corresponding STEM-EDX elemental mapping of products at 10 min.

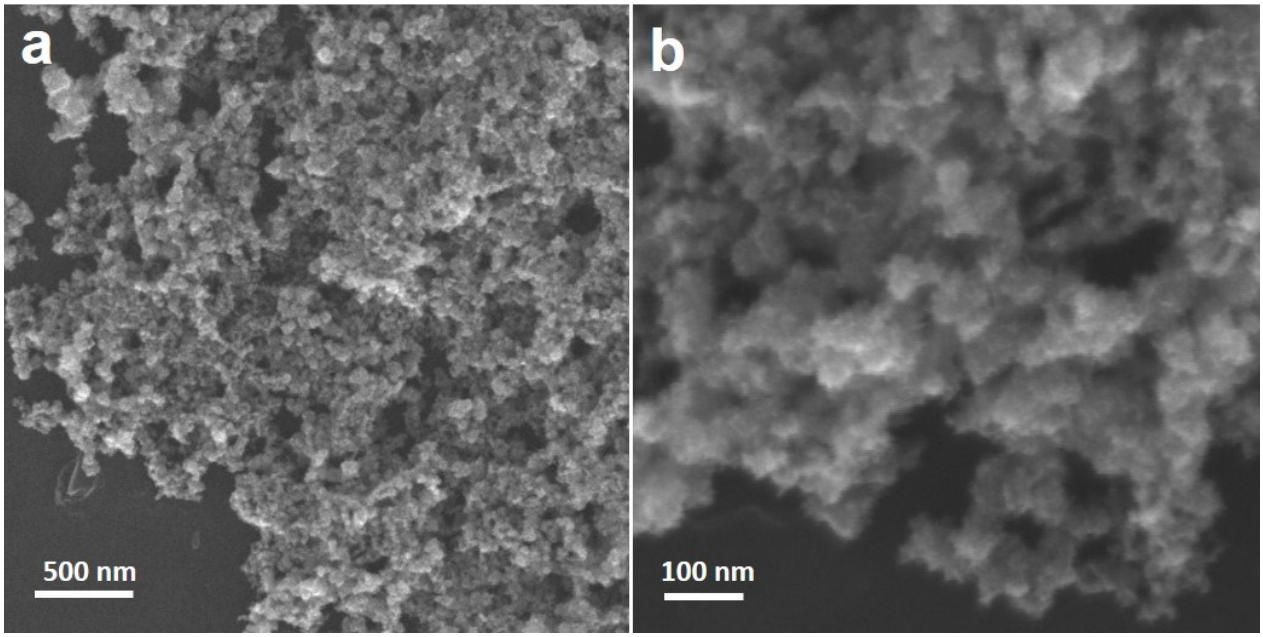

Fig. S8 The SEM image of re-heating the 10 min sample at the typical reaction condition without the metal precursor.

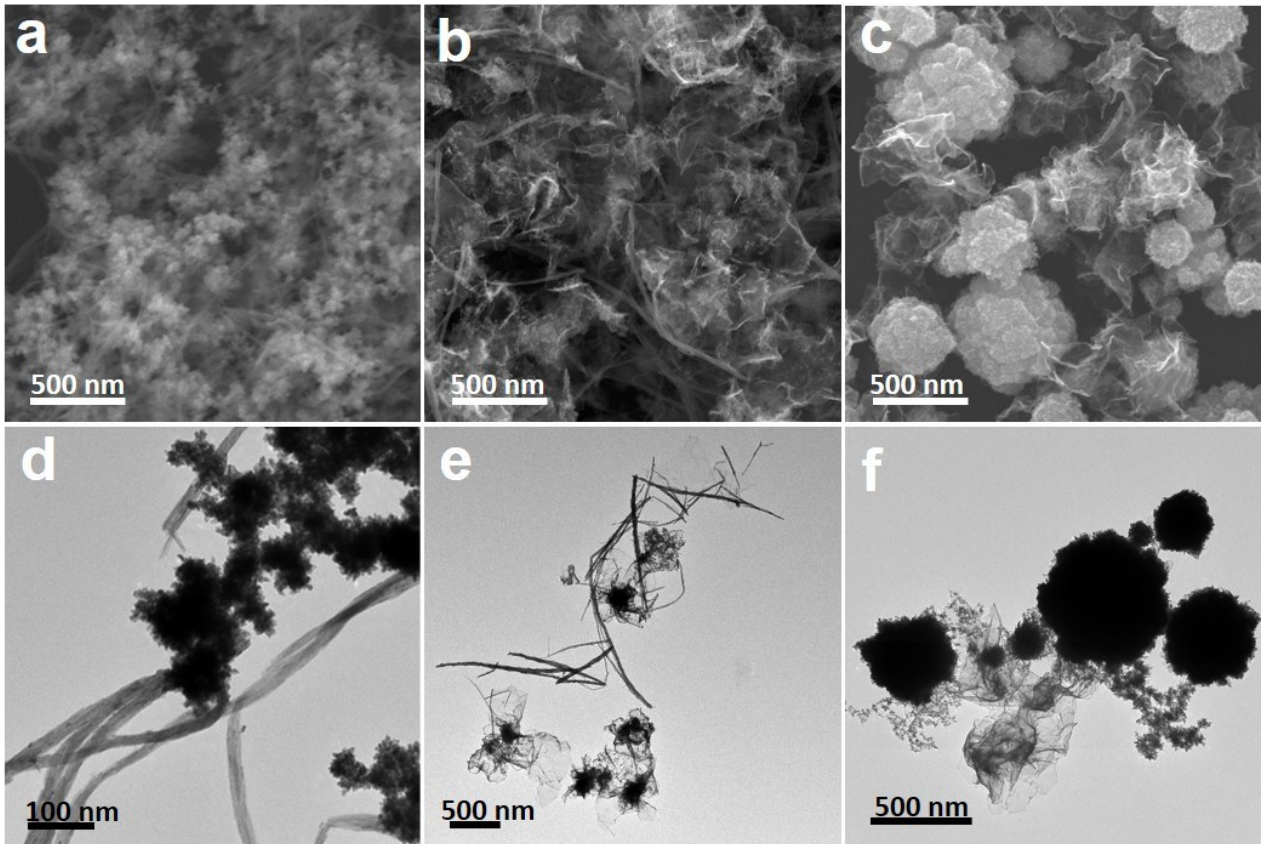

Fig. S9 Representative SEM and TEM images of the products collected from the reaction with the same condition used in the synthesis of Pt-Pd nanosheets but with different amounts of DETA a, d) 0 mL, b, e) 1 mL and c, f) 3mL.

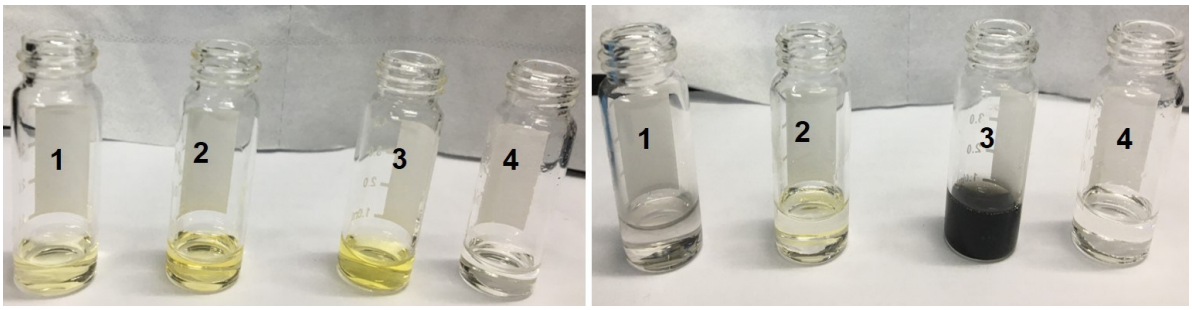

Fig. S10 The color of the solution containing: 1) 10 μL 195 mM H_2PtCl_6 and 0.5 mL H_2O; 2) 10 μL 195 mM H_2PtCl_6 and 0.5 mL DETA; 3) 10 μL 195 mM Na_2PdCl_4 and 0.5 mL H_2O; 4) 10 μL 195 mM Na_2PdCl_4 and 0.5 mL DETA before (left) and 1 min after (right) adding hydrazine hydrate. Sample 1 turned slight greyish in 30s, while sample 2 remain yellow at 10 min. Sample 3 turned black instantly after the addition, while sample 4 slightly darkened after 1min. All of these data showed that DETA could indeed reduce the reduction reaction rate of Pd and Pt precursor.

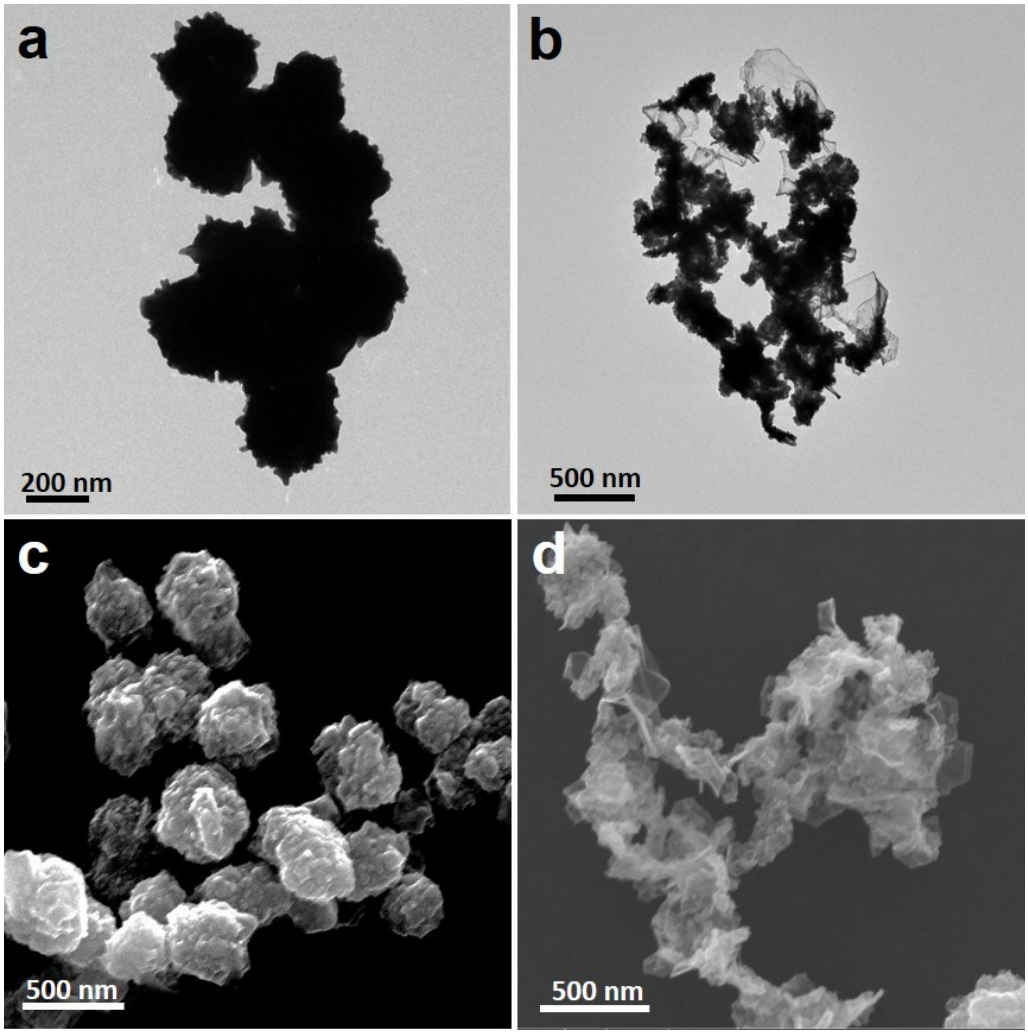

Fig. S11 TEM images at the same condition but at different the amount of KOH: a, c) 0 mg; b, d) 100 mg

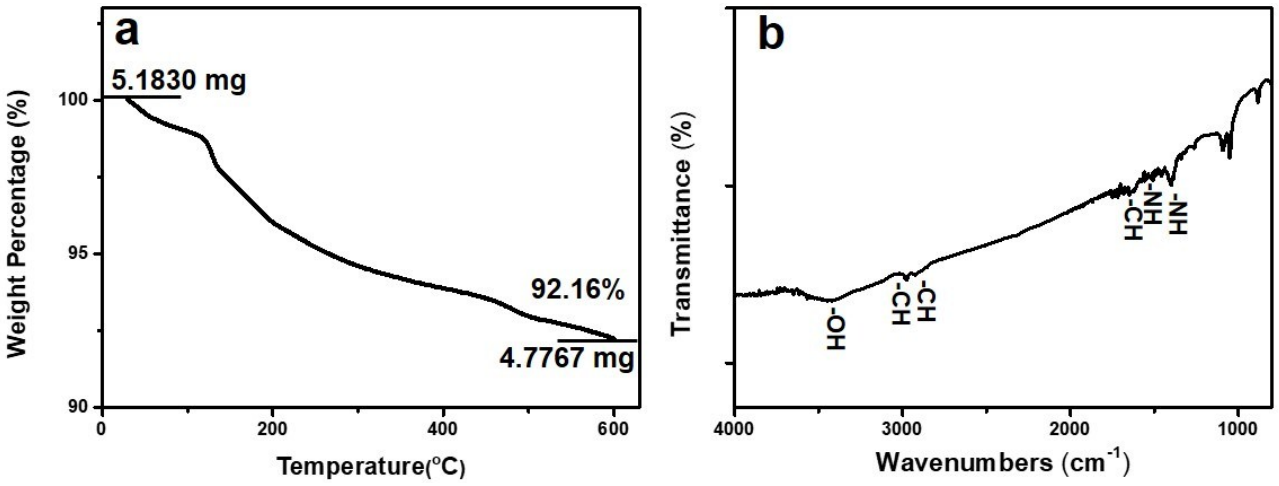

Fig. S12 a) Thermogravimetric analysis (TGA) and b) FT-IR spectrum of samples (at the same reaction condition other than no DETA).

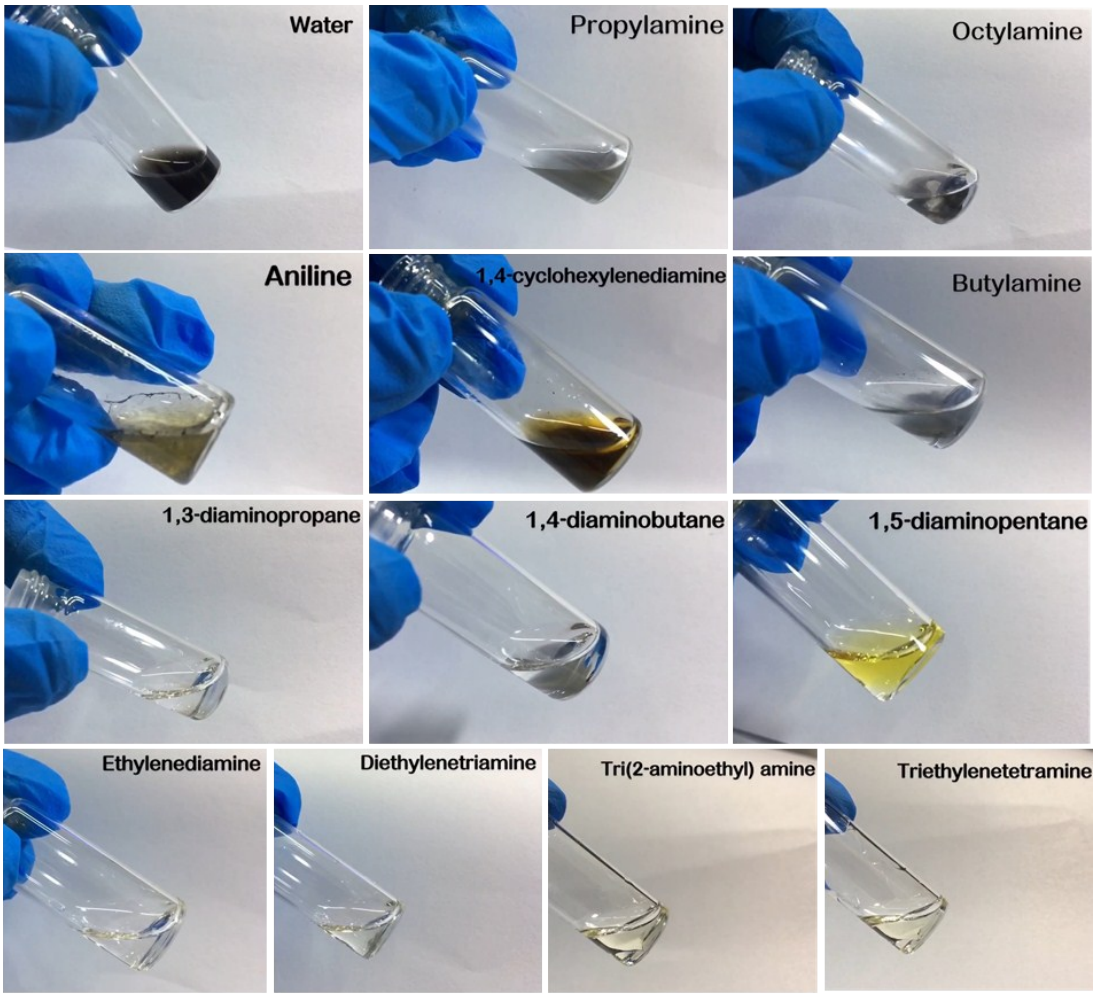

Fig. S13 Digital graphs showing the color change of the $NaPdCl_4$ solution 30s after addition of reductant in the presence of different amine ligands. Without any ligand, the reduction of Pd happened immediately after the addition of reductant in H_2O solution. When aliphatic terminal diamine ligands were added, the reaction mixture remained colorless or pale yellow for a prolonged time (~ 30s), as no reduction occurred. Observable reduction and nucleation happened seconds after addition of reductant when aliphatic terminal monoamine, aromatic amine or cyclic diamine were added.

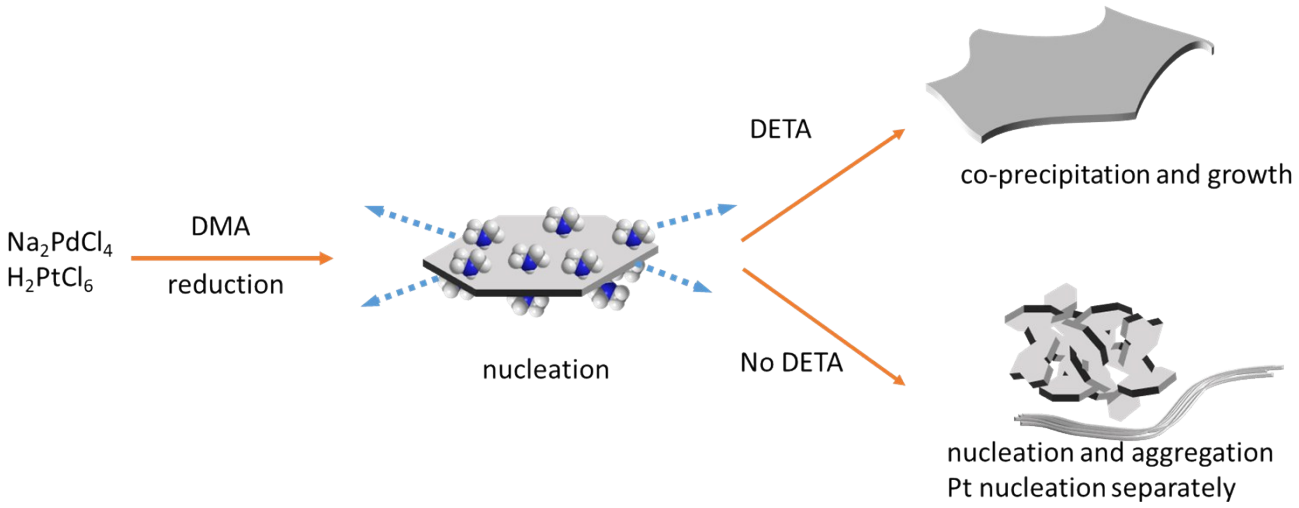

Scheme S1. Schematic illustration for the mechanism of forming Pt-Pd nanosheets.

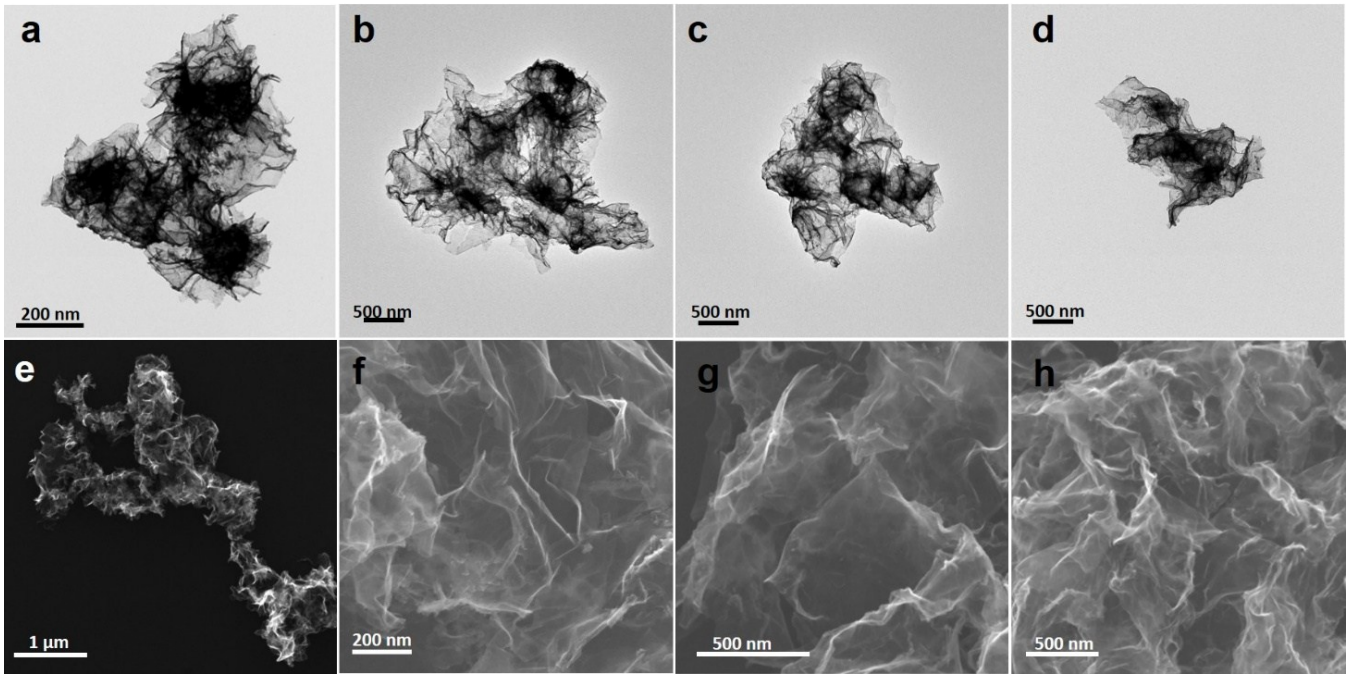

Fig. S14 TEM and SEM images of Pt-Pd alloy nanosheets with different atomic ratios of Pd to Pt. a, e) pure Pd; b, f) 19:1; c, g) 10:1; d, h) 5:1.

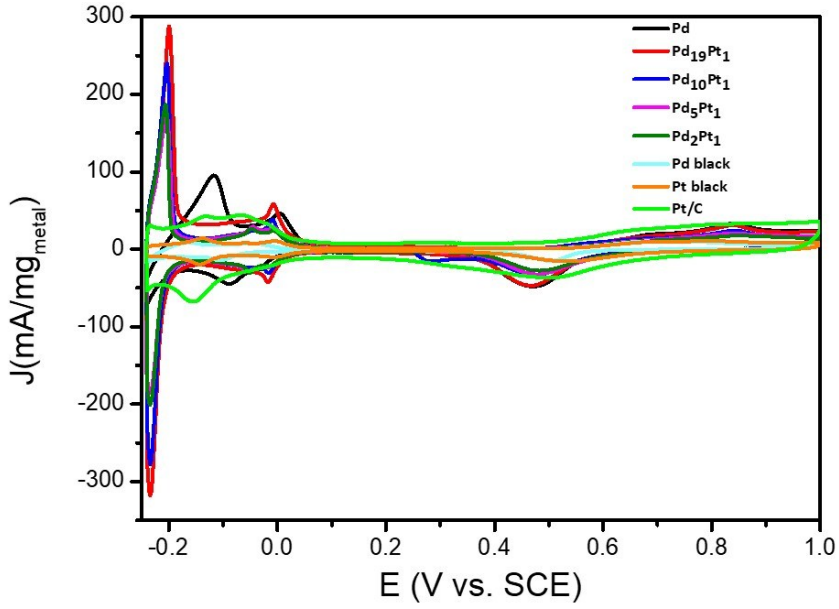

Fig. S15 CV curves of different ratio of Pt-Pd nanosheets and the commercial Pd black, Pt black, Pt/C, recorded in 0.5 M H_2SO_4 aqueous solution at room temperature at scan rate of 50 mV/s.

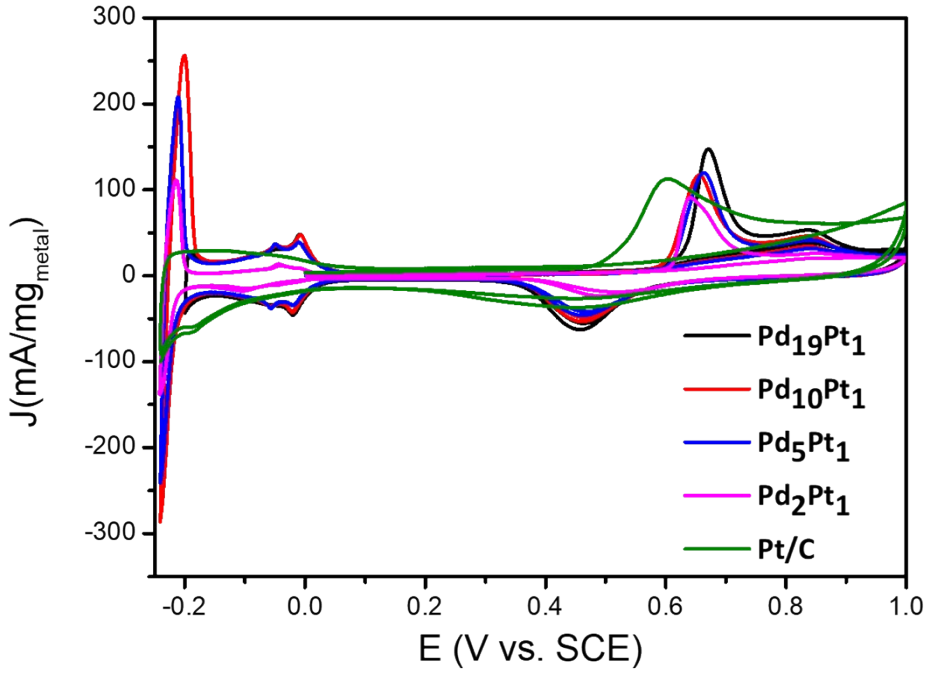

Fig. S16 CO stripping voltammetry of Pt-Pd nanosheets with different Pd/Pt ratios and Pt/C after CO adsorption at 0 V (vs. SCE). Sweep rate 50 mV s^{-1}. Room temperature. The ECSA using CO-stripping were 56, 51.2, 49.2, 35.8, 68.5 m^2/g for $Pd_{19}Pt_1$, $Pd_{10}Pt_1$, Pd_5Pt_1, Pd_2Pt_1, Pt/C. The CO stripping result gives a much smaller area compare to the ECSA for the Pt-Pd nanosheets. This is due to the poor adsorption ability of CO on the Pt-Pd nanosheets surface. Comparing to the Pt surface where the CO usually bond linearly to the surface atom, on PtPd alloy

surface, the CO may take linear, bridged or other manner when bond to the surface Pd. As a result, the CO stripping result would not be reliable[1]. On the other hand, the poor CO adsorption further illustrates the origin of the better FAOR ability of the Pt-Pd nanosheets.

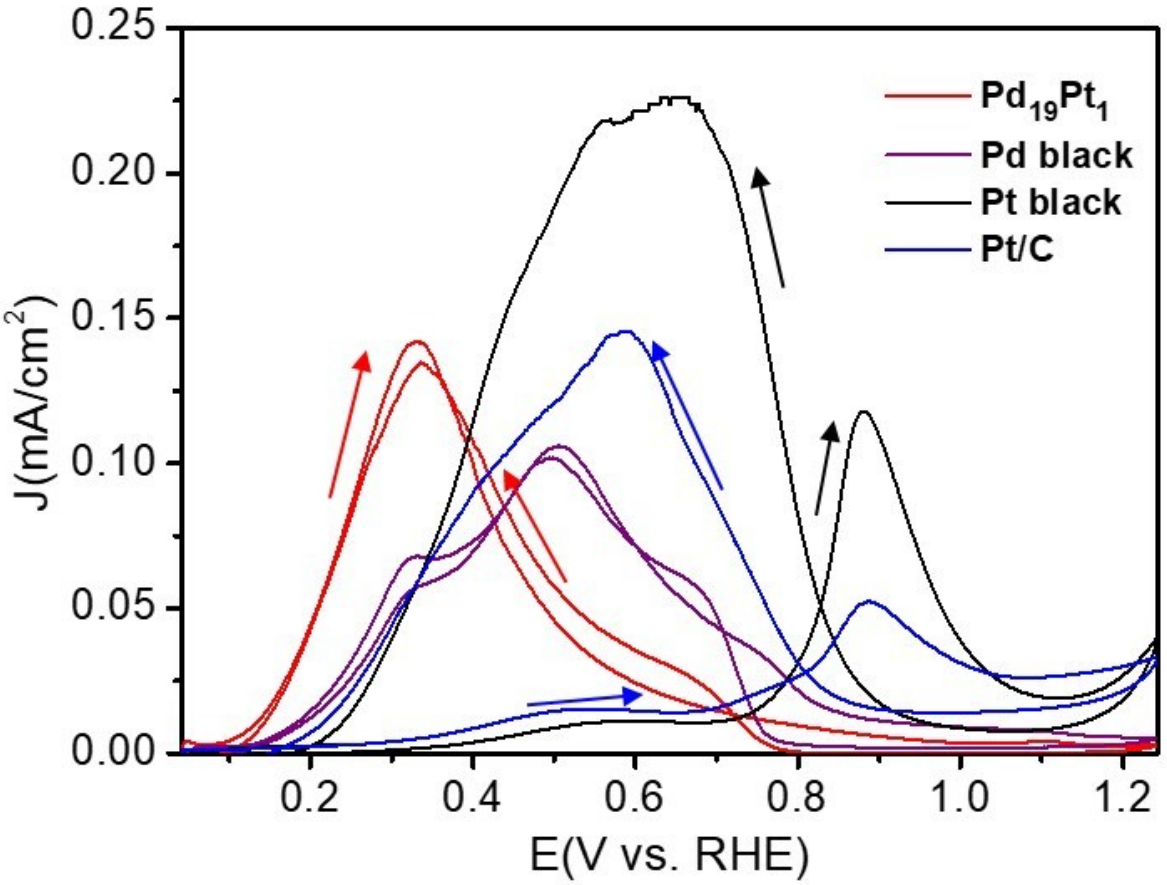

Fig. S17 CV curves of different catalysts towards FAOR in 0.5 M H_2SO_4 and 0.25 M formic acid solution normalized by ECSA.

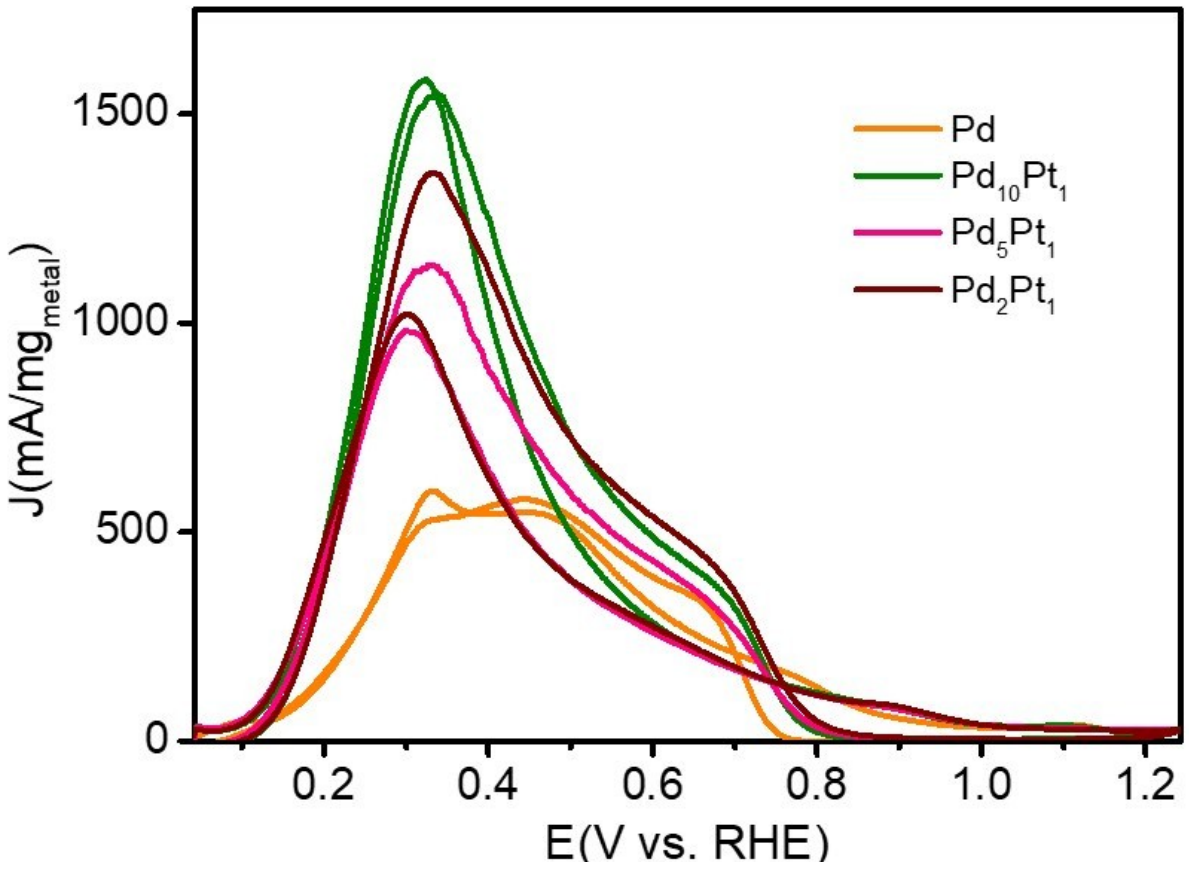

Fig. S18 CV curves of different catalysts in 0.5 M H_2SO_4 and 0.25 M formic acid solution normalized by metal mass at a scan rate of 50 mV s^{-1}.

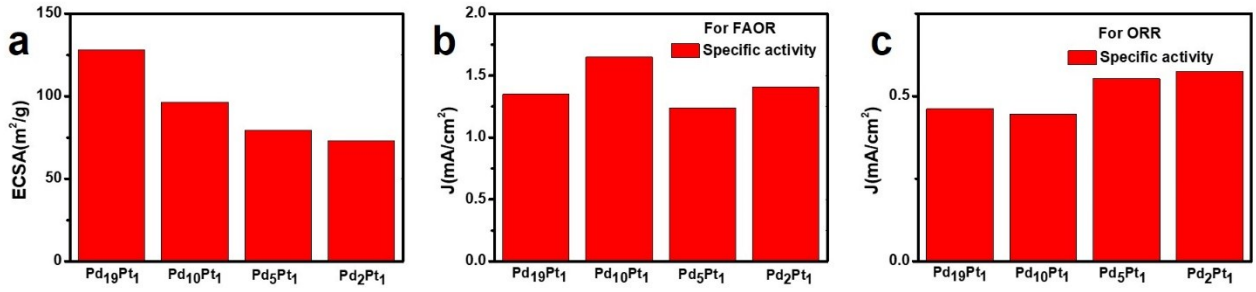

Fig. S19 a) The ECSA, specific activity of b) FAOR and c) ORR of nanosheets with different Pd/Pt ratios.

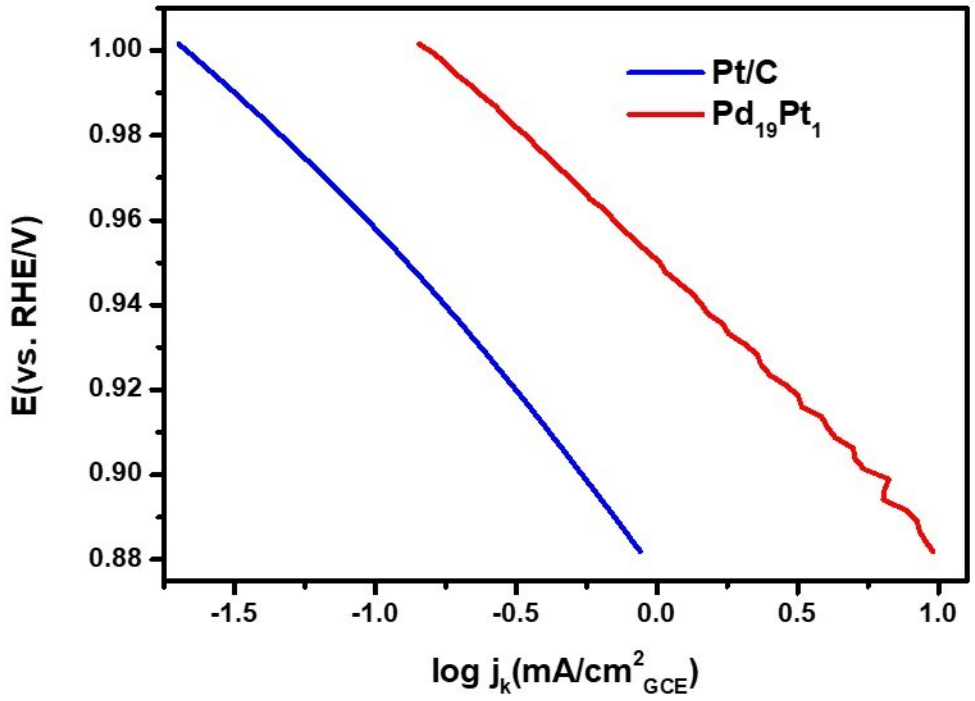

Fig. S20. Tafel plots of $Pd_{19}Pt_1$ nanosheets and Pt/C.

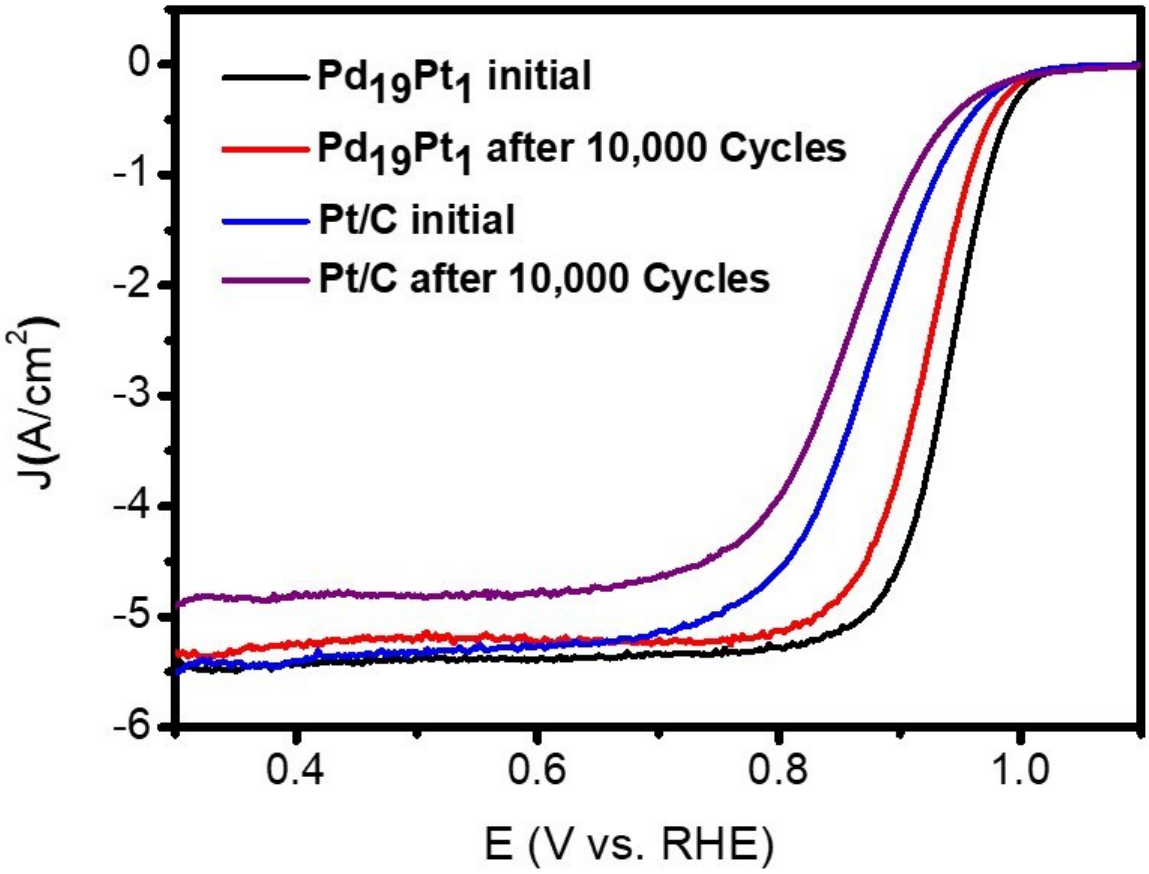

Fig. S21. Electrochemical durability of $Pd_{19}Pt_1$ and commercial Pt/C measured in the range of 0.6 − 1.2 V (vs RHE) at a scan rate of 200 mV s^{-1} in O_2-saturated 0.1 M KOH solution. ORR polarization curves of the $Pd_{19}Pt_1$ catalysts before and after 10,000 potential cycles. The mass activity is 0.25 $A/mg_{(Pd+Pt)}$ and 0.033 $A/mg_{(Pt)}$ for Pt-Pd alloy nanosheets and Pt/C, respectively. After the ADT, the mass activity of Pt-Pd nanosheets is 7.5 times higher than Pt/C in terms of Pd+Pt, showing the better activity and stability of nanosheets.

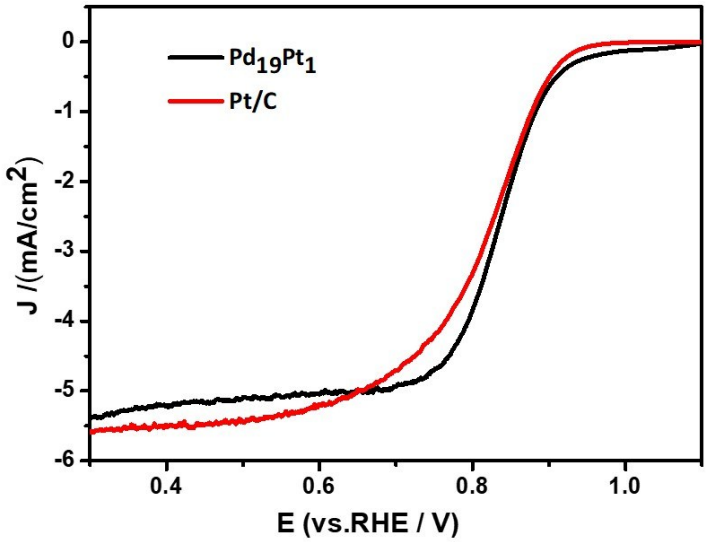

Fig. S22. ORR polarization curves of catalysts in O_2-saturated 0.1 M $HClO_4$ solution and the current density was normalized by the geometric area of GCE.

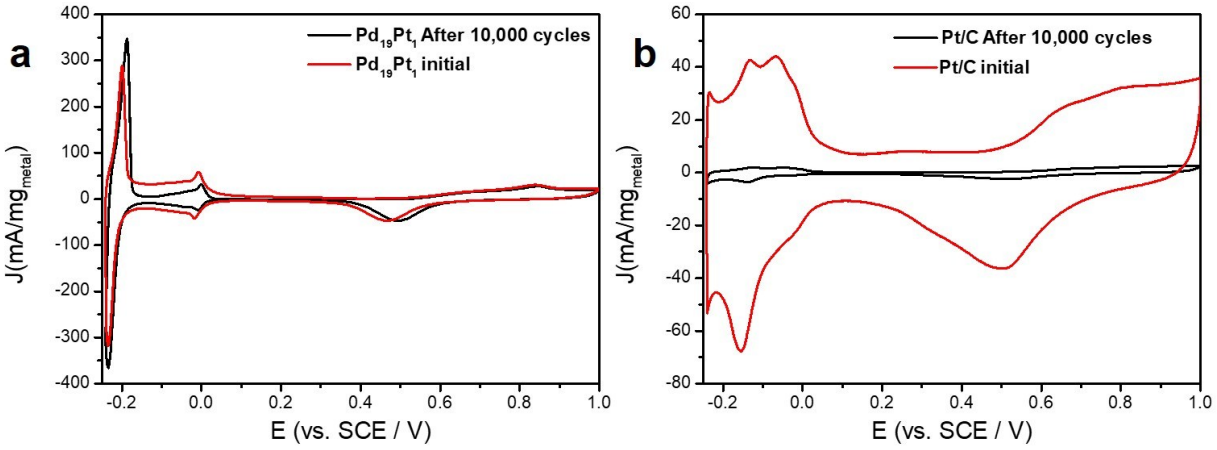

Fig. S23 CV curves of a) Pt-Pd nanosheets and b) Pt/C before and after ADT, recorded in 0.5 M H_2SO_4 aqueous solution at room temperature at scan rate of 50 mV/s. The ECSA of Pt-Pd nanosheets and Pt/C after ADT are 117 m^2/g and 29.9 m^2/g respectively, showing the structure stability of nanosheets.

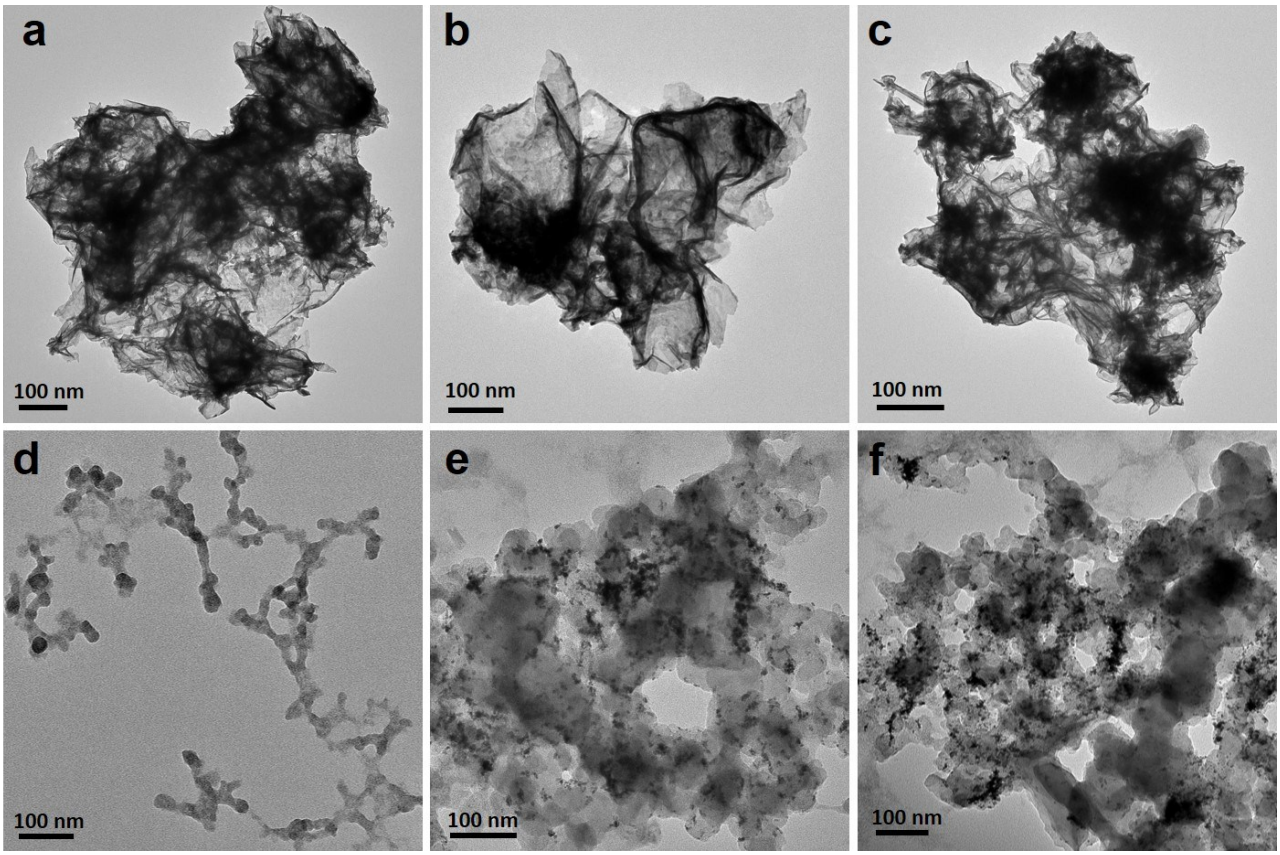

Fig. S24 TEM images of a-c) Pt-Pd nanosheets and d-f) Pt/C after ADT. The nanosheets retained its morphology and structure, while Pt/C occurs agglomeration, ripening and detaching of nanoparticles from carbon carrier. This indicates that the nanosheets have improved stability compared with Pt/C.

Table S1. Comparisons of formic acid activities of ultrathin $Pd_{19}Pt_1$ NSs with those of reported PdPt alloy nanostructures.

catalyst	Mass Activity(A/mg $_{Pd+Pt}$)(FAOR)	Condition	Reference
Carbon nanotubes supported PtPd hollow nanospheres	0.2	0.5M H_2SO_4+0.5M HCOOH	[2]
Nanoporous PdPt nanoparticles	1.29	0.5M H_2SO_4+0.5M HCOOH	[3]
PdPd nanoparticles on carbon nanotube	0.197	0.5M H_2SO_4+0.5M HCOOH	[4]
Pt-Pd-Rh-Ag Nanoframes	1.15	0.5 M H_2SO_4 + 0.25 M HCOOH	[5]
$Pd_{19}Pt_1$ nanosheets	1.831	0.5 M H_2SO_4 + 0.25 M HCOOH	This work

Table S2. Comparisons of ORR activities of ultrathin $Pd_{19}Pt_1$ NSs with recently reported PdPt alloy nanostructures at 0.9 V vs. RHE in 0.1M KOH electrolyte.

catalyst	Mass Activity (A/mg)(ORR)	Condition	Reference
$Pt_{32}Pd_{48}Ni_{20}$ nanosheets	0.54	0.1M KOH	[6]
$Pd_{19}Pt_1$ nanosheets	0.59	0.1M KOH	This work

Reference

1. C. Xu, Q. Hao and H. Duan, *Journal of Materials Chemistry A*, 2014, **2**, 8875.
2. B. Wu, M. Gong, J. Chu, X. Wang, C. Xiao and S. Xiong, *Ionics*, 2015, **21**, 729-736.
3. F. Saleem, B. Ni, Y. Yong, L. Gu and X. Wang, *Small*, 2016, **12**, 5261-5268.
4. J. Lai, F. Lin, Y. Tang, P. Zhou, Y. Chao, Y. Zhang and S. Guo, *Advanced Energy Materials*, 2019, **9**, 1800684.
5. B. Gralec and A. Lewera, *Applied Catalysis B: Environmental*, 2016, **192**, 304-310.
6. B. Liu, H. Y. Li, L. Die, X. H. Zhang, Z. Fan and J. H. Chen, *J. Power Sources*, 2009, **186**, 62-66.